RSC Publishing

COMMUNICATION
Franco Cacialli *et al.*
Micro-focused X-ray diffraction characterization of high-quality [6,6]-phenyl-C$_{61}$-butyric acid methyl ester single crystals without solvent impurities

COMMUNICATION

Micro-focused X-ray diffraction characterization of high-quality [6,6]-phenyl-C_{61}-butyric acid methyl ester single crystals without solvent impurities†

Giuseppe Paternò,[ab] Anna J. Warren,[c] Jacob Spencer,[a] Gwyndaf Evans,[c] Victoria García Sakai,[d] Jochen Blumberger[a] and Franco Cacialli*[ab]

We report the preparation of high-quality, solvent-free [6,6]-phenyl-C_{61}-butyric acid methyl ester (PCBM) large single crystals (size up to 0.5 mm) by slow drying of a chlorobenzene solution at room temperature. The monoclinic structure containing four PCBM molecules per unit cell was successfully solved (*R*-factor = 0.0512) *via* micro-focused X-ray diffraction and employed as a reliable experimental model for further molecular dynamics simulations. We find that the first peak of the simulated fullerene–fullerene radial distribution function is centred at 10.05 Å, giving a nearest neighbour coordination number of 7.0. The work reported herein provides the structural basis for a fundamental understanding of charge transport in this important functional material that is particularly relevant to organic solar cells.

1 Introduction

Achieving large, high-quality, and solvent-free crystals of application-relevant organic semiconductors[1,2] is crucial to affording ever more detailed insights into the fundamental charge and exciton physics underpinning the technology of photovoltaic diodes (PVDs), field-effect transistors (FETs), and light-emitting diodes (LEDs).[3–5] However, this is often far from trivial, not only for high molecular weight materials/polymers such as poly(3-hexylthiophene-2,5-diyl) (P3HT) due to chain entanglement and entropic factors, but also for smaller molecular weight materials such as [6,6]-phenyl-C_{61}-butyric acid methyl ester (PCBM), owing to inclusion of solvent molecules

and/or other impurities. PCBM is a particularly relevant example because it is one of the most popular choices as the electron acceptor in organic solar cells adopting a type-II heterojunction design. Such an architecture is necessary to favour exciton splitting against a substantial exciton binding energy (0.2−1 eV or so),[6] in either bilayer[7] or bulk heterojunction (BHJ) organic solar cells in which the formation of an interpenetrated electron donor–acceptor network has the potential to provide large interface areas and domains that are as close as currently possible to the exciton diffusion range, thereby optimising charge generation.[8,9] Interestingly both amorphous and microcrystalline domains have also been identified in BHJs.[10]

In general, it is thus crucial to understand the physics of charge transport in PCBM in order to optimise this type of solar cells. Despite the large number of papers investigating the morphological and electronic properties of PCBM in solid blends with electron-donor materials,[11–19] a clear understanding of its aggregation behaviour in such a complex system is yet to emerge. Preparation and characterisation of solvent-free crystals have never previously been reported, with the exception of a very recent publication of which we became aware in the final stages of preparation of this manuscript.[20]

Previously, Rispens *et al.* have proved that the solvent choice plays a critical role in the PCBM crystallization behaviour.[21] In particular, when drop-cast from *ortho*-dichlorobenzene (*o*DCB) PCBM was found to form red-brown platelet-shaped crystals with a monoclinic unit cell ($a = 13.76$, $b = 16.63$, $c = 19.08$ Å, and $\beta = 105.3°$), whereas casting from chlorobenzene (CB) leads to the formation of reddish triangle-shaped crystals with a triclinic unit cell ($a = 13.83$, $b = 15.29$, $c = 19.25$ Å, $\alpha = 80.3°$, $\beta = 78.6°$, and $\gamma = 80.41°$). However, regardless of the solvent choice, these authors have noticed solvent inclusion inside the crystals. Furthermore, the substrate nature seems to affect the crystallization pathways undertaken by PCBM. In this context, Dabirian *et al.* prepared crystals *via* dip-coating deposition on three different substrates, observing the formation of crystals with different shapes, namely, hexagonal crystals on silanized SiO_x, amorphous aggregates on graphite and snowflake-like

[a]Department of Physics and Astronomy, University College London, Gower Street, London WC1E 6BT, UK. E-mail: f.cacialli@ucl.ac.uk

[b]London Centre for Nanotechnology, University College London, Gower Street, London WC1E 6BT, UK

[c]Diamond Light Source, Harwell Science and Innovation Campus, Didcot OX11 0DE, UK

[d]ISIS Pulsed Neutron and Muon Source, Science and Technology Facilities Council, Rutherford Appleton Laboratory, Harwell Science and Innovation Campus, Didcot OX11 0QX, UK

† CCDC 942996. For crystallographic data in CIF or other electronic format see DOI: 10.1039/c3tc31075b

This journal is © The Royal Society of Chemistry 2013

J. Mater. Chem. C, 2013, **1**, 5619–5623 | **5619**

crystals on Au.[22] More recently Zheng and Han have prepared hexagonal crystals incorporating solvent molecules *via* liquid–liquid interfacial precipitation.[23] In addition to experimental investigations, various groups have carried out modelling studies to gain insight into the charge transport features and the structure–property relationship in PCBM[24,25], C_{60}[26] and related fullerene derivatives.[27] For this purpose, a reliable and well-defined structure of solvent-free PCBM is required.

Here we report the preparation of high-quality, solvent-free PCBM crystals obtained *via* solvent casting deposition from a chlorobenzene solution, and the XRD characterization *via* the I24 Microfocus Macromolecular Crystallography (MX) beamline at the Diamond Light Source. Our findings will serve as a guide for further experimental and theoretical investigations on PCBM electronic properties.

2 Methods

2.1 Experimental

PCBM was purchased from Aldrich (purity >99%) and used without further purification. The PCBM solution with a concentration of 20 mg ml^{-1} was obtained by dissolving an appropriate amount of PCBM in chlorobenzene (CB) at room temperature. To ensure the complete dissolution of PCBM, the solution was kept stirring overnight at room temperature (295–298 K) in the dark. We obtained PCBM single crystals by placing a droplet (∼100 μL) of the PCBM solution on 15 mm diameter fused silica glass disks at room temperature and allowing the solvent to evaporate. The samples were kept in a capped Petri dish during the deposition and dried under vacuum (∼10^{-2} mbar) overnight to remove the residual solvent. The vacuum treatment was carried out at room temperature. All the preparation procedures were carried out in a nitrogen glove-box to prevent degradation of the material.

XRD measurements were performed on beamline I24 at the Diamond Light Source. The experiment was carried out using an X-ray beam size of 10 μm × 10 μm with a wavelength of 0.62 Å. The sample was held at a temperature of 100 K. The data were processed using *CrysAlis Pro*,[28] the structure was solved with *SHELXS-97*[29] and refined by means of full-matrix least squares in *SHELXL-97*.[29]

2.2 Computation

Molecular dynamics (MD) simulations were carried out for a 3 × 3 × 3 supercell (108 PCBM molecules) using the experimental crystal structure as initial coordinates. Two simulations were run for 100 and 300 K applying periodic boundary conditions. The systems were equilibrated in the NPT ensemble at 1 bar for about 4–11 ns using a Langevin piston with anisotropic pressure rescaling. Thereafter, simulations were carried out in the NVT ensemble at the respective equilibrium densities. Radial distributions and coordination numbers were averaged over 1000 frames taken from a 10 ns MD trajectory in the NVT ensemble. Parameters for bonded and non-bonded interactions were chosen as in ref. 25 *i.e.* OPLS parameter from ref. 30 with C_{60} bond lengths taken from ref. 31. The only exception is the

Lennard-Jones distance parameter for the carbon atoms of the C_{60} cages, which we increased to $\sigma = 3.832$ Å from 3.550 Å in the OPLS force field. The value was adjusted so as to reproduce the experimental density of fcc-C_{60} at room temperature.[32] The integration time step for the MD simulation was 1 fs. The MD simulations were carried out with the NAMD package.[33]

3 Results and discussion

Fig. 1 presents the optical microscopy images of the PCBM crystals produced *via* slow evaporation of the solvent. The best quality crystals were obtained by drop-casting a 20 mg ml^{-1} CB solution on fused silica glass. To obtain a solvent saturated atmosphere and slow down the solvent evaporation dynamics, the samples were placed in a capped Petri dish and kept overnight. Such a deposition technique, with a reduced solvent evaporation rate, enabled the formation of large PCBM crystalline aggregates with a lateral size of up to 500 μm. The preparation procedure involved the optimization of several parameters including solvent, PCBM concentration and substrate.

The images display the presence of high-quality, rhomboidal-shaped crystals, with sizes ranging from ∼10 μm to 260 μm. In particular, Fig. 1a shows a single PCBM crystal (with a top surface ∼260 × 30 μm^2). Some crystals were also found to stack on top of one another (Fig. 1b) or to merge with neighbouring crystals to form round-shaped crystalline aggregates with a radius in the range of ∼40 to 120 μm (Fig. 1c and d). This rectangular prism crystal habit for PCBM seems to be unprecedented, as Rispens[21] and Dabirian[22] have found different shapes for PCBM single crystals. This might be related to the different substrate used in our experiment and, hence, confirms the important role played by the substrate nature in affecting the PCBM crystallization behaviour.

The XRD micro-focus characterization revealed that PCBM assembles into a monoclinic unit cell containing four PCBM molecules (Table 1 and Fig. 2a and b). Remarkably, this structure does not show any solvent inclusion, in contrast to what
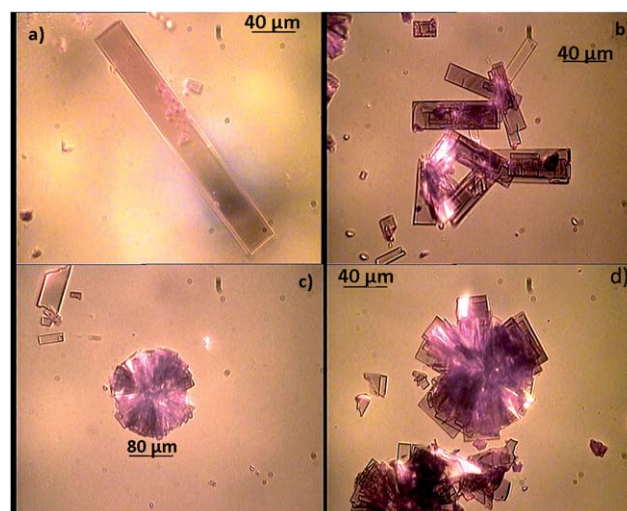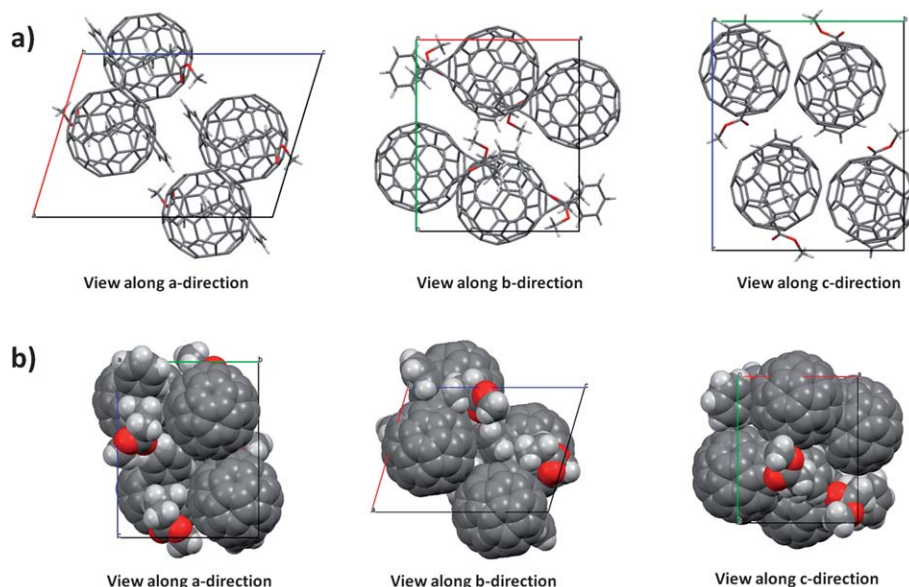

Fig. 1 Optical microscopy images of PCBM crystal solvent cast from CB.

5620 | *J. Mater. Chem. C*, 2013, **1**, 5619–5623

This journal is © The Royal Society of Chemistry 2013

Table 1 XRD data collected at the microfocus beamline

Empirical formula	Crystal system	Space group	Unit cell dimension	Volume	Z	Density	Final R indices
$C_{72}H_{14}O_2$	Monoclinic	$P2(1)/n$	Experimental, 100 K, $a = 13.47$ Å, $\alpha = 90°$, $b = 15.1$ Å, $\beta = 106.90°$, $c = 19.01$ Å, $\gamma = 90°$	3708.70 Å^3	4	1.631 g cm^{-3}	$R_1 = 0.0512$, $wR_2 = 0.1503$
			MD, 100 K, $a = 13.25$, $\alpha = 90°$, $b = 14.77$, $\beta = 106.23$, $c = 19.48$, $\gamma = 90°$	3660.35 Å^3		1.653 g cm^{-3}	
			MD, 300 K, $a = 13.29$, $\alpha = 90°$, $b = 14.93$, $\beta = 106.33$, $c = 19.48$, $\gamma = 90°$	3709.28 Å^3		1.631 g cm^{-3}	

Fig. 2 (a) Monoclinic crystal packing of PCBM along a, b and c directions and (b) van der Waals sphere representation.

was found by Rispens[21] and Zheng.[23] This is corroborated by the considerably smaller unit cell volume reported here as compared to that reported by Rispens (3708.70 Å^3 *vs.* 3984.9 Å^3 for the triclinic and 4210.8 Å^3 for the monoclinic respectively, although this may partly be due to contraction of the crystals at 100 K, the measurement temperature). In addition, a van der Waals sphere representation (Fig. 2b) clearly indicates that there is not enough space to accommodate a solvent molecule inside the unit cell. Good agreement between the calculated crystallographic model and the experimental XRD data is demonstrated by the relatively low value of the R-factor (5.12%).

Classical molecular dynamics simulations of the solvent-free monoclinic PCBM crystal have been carried out for the temperature at which the X-ray structure was solved (100 K) and for room temperature (300 K), see the Methods section for simulation details. The unit cell parameters obtained are summarized in Table 1. We find that the molecular model predicts the equilibrium density at 1 bar and 100 K reasonably well, overestimating the experimental value by only 1.3%. From the finite difference of the simulated volumes at 100 and 300 K we estimate a thermal expansion coefficient of 6.7×10^{-5} K^{-1}, which is similar to the experimental value for C_{60}, 6.2×10^{-5} K^{-1}.[32]

The thermal fluctuations of the fullerene molecules are characterized in more detail by computing the centre-to-centre radial distribution functions of the C_{60} cages, shown in Fig. 3. The first peak is centred at 10.05 ± 0.10 Å (100 K) and ranges from 9.55 to 10.55 Å, matching closely the shortest distances in the crystal structure (9.56–10.85 Å, indicated by dashed spikes). The second peak exhibits a shoulder at 12.75 Å and a maximum at 13.25 Å matching again closely the discrete distances in the crystal structure. When the temperature is increased to 300 K the position of the first maximum remains virtually unchanged, and the shoulder at larger distances merges into a single broad peak centred at 12.95 Å. Thus, at room temperature the average nearest neighbour distance in monoclinic PCBM, 10.05 Å, is within statistical errors identical to the distance in fcc-C_{60} (10.02 Å using a lattice constant of 14.17 Å at 300 K (ref. 32)).

Coordination numbers (CN) were obtained by spherical integration of the radial distributions, shown as insets in Fig. 3. Integration up to the first minimum at 11.0 Å gives a CN of 7.0 and further integration up to the second minimum at 13.8 Å gives a CN of 12.0. As can be seen, the CNs are rather insensitive to temperature in the range of 100–300 K. We note that the nearest neighbour CN (7.0) is higher than previously reported
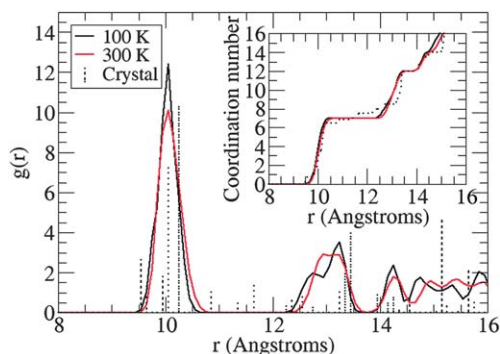
Fig. 3 Radial distribution function of solvent-free monoclinic PCBM as obtained from classical molecular dynamics simulation at 100 and 300 K. The spectra of discrete distances in the X-ray structure are shown as dashed spikes. The distance r is the separation between the centres of mass of the C_{60} cages of PCBM. Coordination numbers are shown in the inset.

values for monoclinic PCBM which contained solvent impurities (PCBM : ODCB = 1 : 1, CN = 6), but similar to the one reported for triclinic PCBM, where the PCBM to solvent ratio was higher (PCBM : CB = 2 : 1, CN = 7).[21,34]

4 Conclusion

We have reported the preparation and micro-focused XRD structural characterisation of large and high-quality crystals of PCBM. These provide a much needed experimental validation for computational models that build on such structural information for analysis and prediction of photophysical and charge transport properties in this class of materials. The results are highly relevant to applications such as solar cells, field-effect transistors, and more generally for organic and plastic electronics. While in the final stages of preparation of this manuscript we became aware of similar results obtained by Casalegno and collaborators,[20] who also obtained solvent-free crystals but with a slightly different procedure, that involved the use of a different solvent and heating the crystals, instead of simply exposing them to vacuum. Such a concomitant and independent finding that it is indeed possible to prepare solvent-free crystals disproves the long-held and discouraging belief that it is impossible to obtain solvent-free crystals of PCBM. In turn, it fully validates the selection of this material as both an experimental and computational model for charge transport and photophysical studies. Our good agreement between experimental and computed structures, as evidenced by radial distributions and thermal expansion coefficient, suggests that the present atomistic model is especially well-suited for future investigations of electron transport in this important material.

Acknowledgements

References

1 B. Fraboni, C. Femoni, I. Mencarelli, L. Setti, R. Di Pietro, A. Cavallini and A. Fraleoni-Morgera, *Adv. Mater.*, 2009, **21**, 1835–1838.

2 A. Fraleoni-Morgera, L. Benevoli and B. Fraboni, *J. Cryst. Growth*, 2010, **312**, 3466–3472.

3 V. Podzorov, *MRS Bull.*, 2013, **38**, 15–27.

4 A. L. Briseno, S. C. Mannsfeld, M. M. Ling, S. Liu, R. J. Tseng, C. Reese, M. E. Roberts, Y. Yang, F. Wudl and Z. Bao, *Nature*, 2006, **444**, 913–917.

5 A. A. Virkar, S. Mannsfeld, Z. Bao and N. Stingelin, *Adv. Mater.*, 2010, **22**, 3857–3875.

6 J. L. Brédas, J. Cornil and A. J. Heeger, *Adv. Mater.*, 1996, **8**, 447–452.

7 A. L. Ayzner, C. J. Tassone, S. H. Tolbert and B. J. Schwartz, *J. Phys. Chem. C*, 2009, **113**, 20050–20060.

8 G. Yu and A. J. Heeger, *J. Appl. Phys.*, 1995, **78**, 4510–4515.

9 J. J. M. Halls, C. A. Walsh, N. C. Greenham, E. A. Marseglia, R. H. Friend, S. C. Moratti and A. B. Holmes, *Nature*, 1995, **376**, 498–500.

10 W. Yin and M. Dadmun, *ACS Nano*, 2011, **5**, 4756–4768.

11 X. N. Yang, J. K. J. van Duren, M. T. Rispens, J. C. Hummelen, R. A. J. Janssen, M. A. J. Michels and J. Loos, *Adv. Mater.*, 2004, **16**, 802–806.

12 H. Hoppe, A. Drees, W. Schwinger, F. Schaffler and N. S. Sariciftci, *Synth. Met.*, 2005, **152**, 117–120.

13 X. N. Yang, J. K. J. van Duren, R. A. J. Janssen, M. A. J. Michels and J. Loos, *Macromolecules*, 2004, **37**, 2151–2158.

14 H. Hoppe, T. Glatzel, M. Niggemann, A. Hinsch, M. Lux-Steiner and N. S. Sariciftci, *Nano Lett.*, 2005, **5**, 269–274.

15 F. Piersimoni, S. Chambon, K. Vandewal, R. Mens, T. Boonen, A. Gadisa, M. Izquierdo, S. Filippone, B. Ruttens, J. D'Haen, N. Martin, L. Lutsen, D. Vanderzande, P. Adriaensens and J. V. Manca, *J. Phys. Chem. C*, 2011, **115**, 10873–10880.

16 A. Swinnen, I. Haeldermans, M. vande Ven, J. D'Haen, G. Vanhoyland, S. Aresu, M. D'Olieslaeger and J. Manca, *Adv. Funct. Mater.*, 2006, **16**, 760–765.

17 M. Reyes-Reyes, R. Lopez-Sandoval, J. Arenas-Alatorre, R. Garibay-Alonso, D. L. Carroll and A. Lastras-Martinez, *Thin Solid Films*, 2007, **516**, 52–57.

18 L. Li, G. Lu, S. Li, H. Tang and X. Yang, *J. Phys. Chem. B*, 2008, **112**, 15651–15658.

19 M. Dante, J. Peet and T. Q. Nguyen, *J. Phys. Chem. C*, 2008, **112**, 7241–7249.

20 M. Casalegno, S. Zanardi, F. Frigerio, R. Po, C. Carbonera, G. Marra, T. Nicolini, G. Raos and S. Meille, *Chem. Commun.*, 2013, **49**, 4525–4527.

5622 | *J. Mater. Chem. C*, 2013, **1**, 5619–5623

This journal is © The Royal Society of Chemistry 2013

21 M. T. Rispens, A. Meetsma, R. Rittberger, C. J. Brabec, N. S. Sariciftci and J. C. Hummelen, *Chem. Commun.*, 2003, 2116–2118.

22 R. Dabirian, X. Feng, L. Ortolani, A. Liscio, V. Morandi, K. Müllen, P. Samorì and V. Palermo, *Phys. Chem. Chem. Phys.*, 2010, **12**, 4473–4480.

23 L. Zheng and Y. Han, *J. Phys. Chem. B*, 2012, **116**, 1598–1604.

24 F. Gajdos, H. Oberhofer, M. Dupuis and J. Blumberger, *J. Phys. Chem. Lett.*, 2013, **4**, 1012–1017.

25 D. L. Cheung and A. Troisi, *J. Phys. Chem. C*, 2010, **114**, 20479.

26 H. Oberhofer and J. Blumberger, *Phys Chem. Chem. Phys.*, 2012, **14**, 13846.

27 R. C. I. MacKenzie, J. M. Frost and J. Nelson, *J. Chem. Phys.*, 2010, **132**, 064904.

28 Agilent (2012). *CrysAlis Pro*. Agilent Technologies, Yarnton, Oxfordshire, England.

29 G. M. Sheldrick, *Acta Crystallogr. Sect. A*, 2008, **64**, 112.

30 W. L. Jorgensen, D. S. Maxwell and J. Tirado-Rives, *J. Am. Chem. Soc.*, 1996, **118**, 11225.

31 K. Hedberg, L. Hedberg, D. S. Bethune, C. A. Brown, H. C. Dorn, R. D. Johnson and M. De Vries, *Science*, 1991, **254**, 410.

32 P. A. Heiney, *J. Phys. Chem. Solids*, 1992, **53**, 1333.

33 J. C. Phillips, R. Braun, W. Wang, J. Gumbart, E. Tajkhorshid, E. Villa, C. Chipot, R. D. Skeel, L. Kale and K. Schulten, *J. Comput. Chem.*, 2005, **26**, 1781.

34 F. Frigerio, M. Casalegno, C. Carbonera, T. Nicolini, S. V. Meille and G. Raos, *J. Mater. Chem.*, 2012, **22**, 5434.

This journal is © The Royal Society of Chemistry 2013

J. Mater. Chem. C, 2013, **1**, 5619–5623 | **5623**